Pierre Pontarotti *Editor*

Evolutionary Biology—A Transdisciplinary Approach

Springer

Pierre Pontarotti
Editor

Evolutionary Biology—A Transdisciplinary Approach

Springer

Editor
Pierre Pontarotti
IHU Marseille MEPHI
Aix Marseille Univ IRD, APHM
Marseille, France

SNC5039 CNRS
Paris, France

ISBN 978-3-030-57245-7 ISBN 978-3-030-57246-4 (eBook)
https://doi.org/10.1007/978-3-030-57246-4

This Springer imprint is published by the registered company Springer Nature Switzerland AG
The registered company address is: Gewerbestrasse 11, 6330 Cham, Switzerland

Contents

Chapter 8
On the Origin of Life and Evolution of Living Systems from a World of Biological Membranes

Aditya Mittal, Suneyna Bansal, and Anandkumar Madhavjibhai Changani

Abstract The central dogma, i.e. DNA to RNA to protein, is central to biology. Biological membranes are also central to biology. However, discussions on origin of life and evolution of living systems rely primarily on nucleic acids and proteins. A contextual appreciation of biological membranes in evolutionary biology has not yet emerged. One of the primary reasons for this is the replication mechanism offered via DNA and its subsequent transcription and translation. In this work, we explore the possibility of a replication mechanism in nucleic acid-free and protein-free self-assembled systems based on the law of mass action. While exploring the role of water, both as a chemical reactant and as a solvent, we present the view of a "micellar world" towards understanding origin of life and subsequent evolution through a thought experiment that we call Life of Micellar Systems (LoMS). We hope that the ideas presented will stimulate discussions on biological membranes towards building completely new perspectives not only in evolutionary biology but also in synthetic biology.

A. Mittal (✉) · S. Bansal · A. M. Changani
Kusuma School of Biological Sciences, Indian Institute of Technology Delhi (IIT Delhi), Hauz Khas, New Delhi 110016, India
e-mail: amittal@bioschool.iitd.ac.in

A. Mittal
Kusuma School of Biological Sciences and Supercomputing Facility for Bioinformatics & Computational Biology, IIT Delhi, Hauz Khas, New Delhi 110016, India

S. Bansal
NIIT Technologies Limited, Tech Zone IT City, Greater Noida, Uttar Pradesh, India

A. M. Changani
Growth Source Financial Technologies, Mumbai, Maharashtra, India

P. Pontarotti (ed.), *Evolutionary Biology—A Transdisciplinary Approach*,
https://doi.org/10.1007/978-3-030-57246-4_8

8.1 Biological Membranes and Evolutionary Biology

Biological membranes are central to biology. Starting from the fluid mosaic model (Singer and Nicolson 1972) to the modern description of biological membranes as two-dimensional fluids with domains/rafts of varying sizes (Brown and London 1998), the overall view of biological membranes has evolved over the years. From a perspective of simply serving as semi-permeable boundaries for whole cells and their intracellular compartments, it is now well-appreciated that there are several key roles played by lipid constituents in biological membranes—for example, molecular recognition, signalling, trafficking and subcellular (re)organization have been discovered in the last couple of decades (see introduction in Bansal and Mittal 2013). However, when it comes to discussions on origin of life and evolution of living systems, biological membranes almost do not find a comprehensive mention. Such discussions are essentially dominated by (self) catalyzing RNA and/or proteins (Deamer 2019). This is because the hallmark of living systems is considered to be the intracellular operation of the central dogma (DNA to RNA to protein)—biological membranes do not feature in the central dogma. Thus, in spite of availability of abundant literature on the informatics of nucleic acids and proteins, "lipidomics" is mostly addressed in literature in terms of enzymes that carry out (bio) chemical transformations resulting in formation of lipids. In one of the first analyses inspired by computational genomics and proteomics, a model for the origin of eukaryotic cells was developed based on membrane lipidomics on three domains of life—a unique lipid class diagram was developed for classifying thousands of lipids that constitute biological membranes in all the three domains of life (Bansal and Mittal 2015). Subsequently, analyses of thickness of subcellular biological membranes allowed development of some interesting novel insights into origins and evolution of cellular and multi-cellular life forms (Singh and Mittal 2016; Mittal and Singh 2018). However, evolutionary biology is still far away from giving considerations to biological membranes in comparison with nucleic acids and proteins.

From invention of optical microscopy up to mid-twentieth century, erythrocytes (red blood cells—RBCs), in addition to having their own significance in clinical and basic biology, have served as model systems for insights into behaviour of biological membranes (Singh et al. 2019). Subsequently, liposomes have served as a promising model system for understanding biological membranes for the last half-a-century. However, there is only one report till date that experimentally derives a quantitative formalism called the "Critical Compartmentalization Concentration" for stoichiometric assembly of amphipathic molecules into aggregating assemblies of a given size that serve as compartments (Mittal and Grover 2010). In contrast, assembly of micelles from amphipathic molecules is extremely well covered in the literature, largely owing to the pioneering work of Tanford (1973, 1978) on the hydrophobic effect. Micellar aggregation also serves as a model system towards gaining insights into formation and behaviour of biological membranes. Thus, in this chapter, we propose a completely new model for the origin of life and evolution of living systems based entirely on micellar systems. By carrying out a thought experiment called

"Life of Micellar Systems" (LoMS), we propose a "micellar world" for origin of life and evolution of living systems rather than a primarily "protein" and/or "RNA" world. We are hopeful that the ideas presented will stimulate discussions on biological membranes from a completely new perspective contributing towards not only evolutionary biology but also synthetic biology.

The Life of Micellar Systems (LoMS) "thought" experiment Here we discuss the origin of life and evolution of living systems from a "Micellar World". Consider a system shown in the leftmost panel of Fig. 8.1.

Micelle forming amphiphiles (denoted by "*X*"), with a hydrophilic head group and a hydrophobic chain, are suspended in a given amount of water—water serves primarily as the solvent. As per the law of mass action, aggregation of *X* resulting in a micelle is shown by the equation given at the top of Fig. 8.1—a key assumption, for simplification, here is that there are only two possible thermodynamic states in which the molecular species "*X*" can exist: either a monomer or a micelle (no other aggregate is considered to be either thermodynamically favourable or have any kinetic lifetime to be of any consequence). Further, assume that the aggregation number of

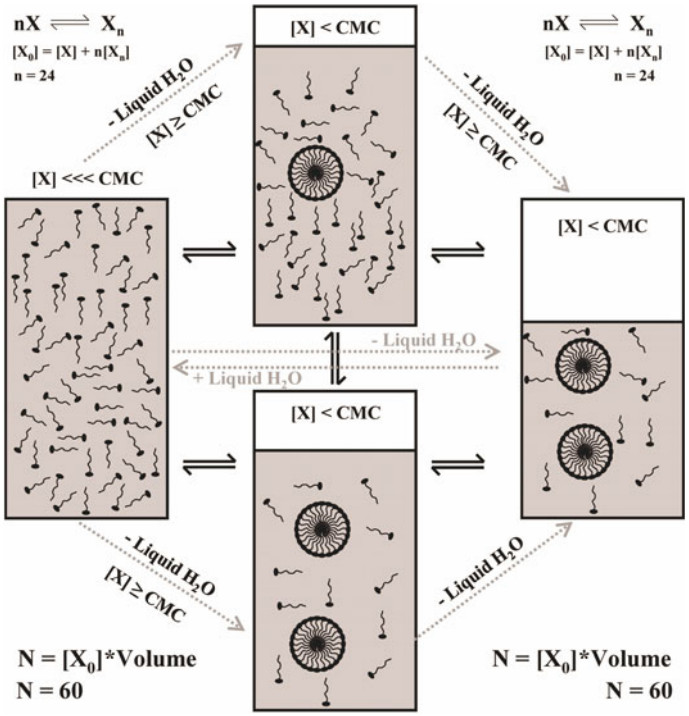

Fig. 8.1 Birth of a micelle—aggregation of amphiphiles in water and apparent "replication" of aggregates by law of mass action. The mass balance on *X* is given by $N = [Xo] * \text{Volume}$, where $[Xo] = [X] + n[Xn]$

X, denoted by "n", is 24 (i.e. formation of a micelle requires exactly 24 molecules of X). Total number of X molecules in the system, denoted by "N", is 60 and remains constant. In the leftmost panel of Fig. 8.1, the concentration of monomeric X, given by $[X]$, is much lower than the critical micellar concentration (CMC), i.e. $[X] \lll$ CMC. Now, let us remove some water from the system—the top middle panel in Fig. 8.1 shows the formation of single micelle transiently due to the concentration of X reaching the threshold of CMC due to the removal of water—here it is important to note that removal of water as a solvent is not to be confused with "dehydration" of the micelles; dehydration at a molecular level results in conformational alterations and changes in aggregation patterns. In fact, it is well known that bulk water properties (water serving as a solvent) are significantly different from the properties of water that form the hydration layers in the self-assembled structures.

A little more removal of water, shown by the bottom middle panel in Fig. 8.1, shows the formation of two micelles transiently—in both these systems, there is an equilibrium between X (monomers) and Xn (micelles), depending on the amount of water in the system. Note that since $n = 24$ and $N = 60$, at most two micelles are formed in this system. Now, further the removal of water from the system, as shown by the rightmost panel in Fig. 8.1, will not affect the equilibrium between the two micelles and the monomers. Thus, we have observed the spontaneous "birth of a micelle" in a system simply by the manifestation of the law of mass action in a system where the quantity of water as a solvent is varied. Note that the transitions shown by only removal or addition of water, and maintenance of $N = 60$ in the system, are all reversible due to the law of mass action with corresponding addition or removal of water. However, in very dilute conditions, i.e. if $[X] \lll$ CMC, no micelle will ever form (as in leftmost panel). Similarly, at high concentration of X (but N still $= 60$) due to the removal of sufficient water, two micelles will always be at equilibrium with 12 monomeric X (since $n = 24$). Clearly, this not only provides a direct analogy to spontaneous appearance of a single self-assembled system ("birth of a micelle") further leading to appearance of "replication" resulting in appearance of two similar (in this case identical) self-assembled systems simply by controlling water volume. Now consider a system shown in the leftmost panel of Fig. 8.2.

All of the system characteristics are exactly the same as those in Fig. 8.1, except that $N = 48$ in this system (instead of $N = 60$ as in Fig. 8.1). Therefore, here the total number of X molecules in the system is 48 and remains constant. Again, the leftmost panel of Fig. 8.2 shows that the concentration of monomeric X, given by $[X]$, is much lower than the critical micellar concentration (CMC), i.e. $[X] \lll$ CMC. Now, removal of some water from the system, as shown in the top middle panel of Fig. 8.2, results in formation of single micelle transiently due to the concentration of X reaching the CMC threshold. A little more removal of water, shown by the bottom middle panel in Fig. 8.2 shows the formation of two micelles; however, micelle formation is not transient in both the systems this time. This is because the number of monomers is an exact multiple of the aggregation number of the monomer; hence, once the energetically favourable micellar configuration is reached for all monomers (i.e. micelles formed do not disaggregate—this results in disappearance of monomers). Of course, the law of mass action may now manifest itself via exchange of amphiphilic

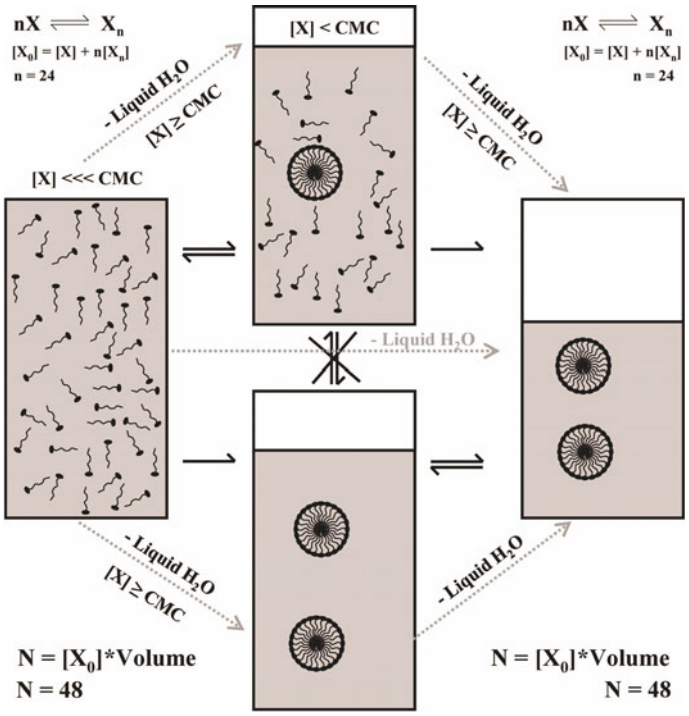

Fig. 8.2 Life of a micelle—aggregation of amphiphiles in water, the illusion of replication and lifespan of aggregates in a "stagnant" system. The mass balance on X is given by $N = [Xo] *$ Volume, where $[Xo] = [X] + n[Xn]$

molecules between the two micelles in the bottom middle panel; however, there will be no remaining monomeric species. Thus, there is a clear distinction in this case from that shown in Fig. 8.1—while there is an equilibrium between X and Xn in the top middle panel, the bottom middle panel represents a stable and irreversible micellar system with complete absence of monomers. Further, the removal of water (shown in the rightmost panel) or even further addition of water to the system in the bottom middle panel will not affect the system since the micellar aggregates are energetically stable. These observations can be specifically noted by contrasting the reversibility versus irreversibility of the systems, represented by reaction directions, in Figs. 8.1 and 8.2. Thus, here we have observed not only the spontaneous "birth and replication of micelles" but also "lifespan of micelles". This lifespan of the micelles will continue until (a) there is an energetic epoch in the system to destabilize one or both of the micelles, or (b) there is another molecular species that can interact with X is introduced in the system that can have an "interaction constant" (e.g. binding affinity) to extract X out of either or both micelles, or (c) there is an introduction of more X molecules in order to re-invoke the law of mass action-driven equilibrium between monomers and micelles. Until such perturbations are introduced in the system, the

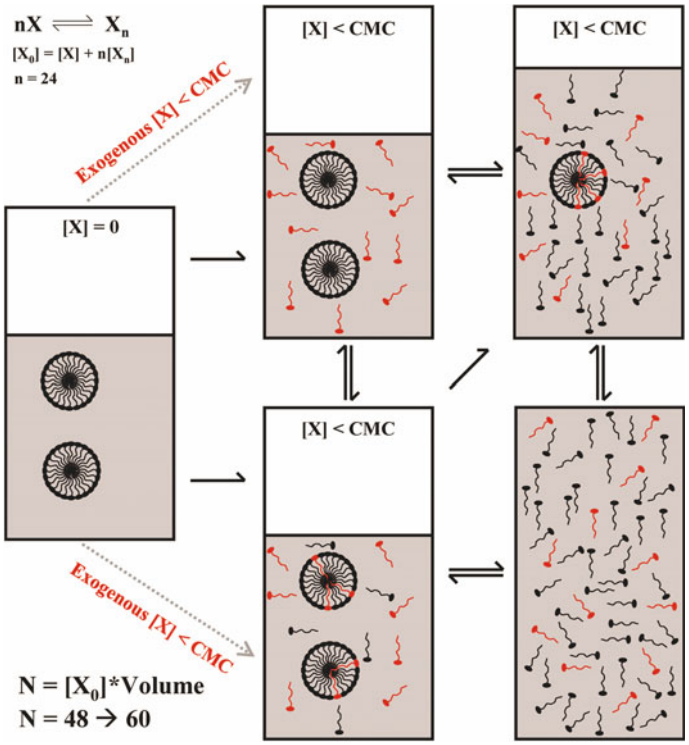

Fig. 8.3 Death of micelles—Disaggregation of stable micelles due to perturbations. The mass balance on X is given by $N = [Xo] * \text{Volume}$, where $[Xo] = [X] + n[Xn]$

two micelles will apparently "live happily forever after". Now, let us introduce one of the perturbations discussed above—the simplest one being introduction of more X monomers in the system. Figure 8.3 shows addition of more monomeric X molecules in the "living system" shown in the leftmost panel. The "living system" has $N = 48$ (same as in Fig. 8.2), and 12 more monomers are added to bring the total molecules of X to $N = 60$ (same as in Fig. 8.1). For clarity, the new X monomers are shown in red, compared to the original black. Without any change in the amount of water, the system will be driven towards equilibrium between monomers and micelles driven by the law of mass action. Now, after addition of the new monomers, further addition of water will result in dilution of the system and at some point when $[X] \lll$ CMC, the system will resemble the original starting system in Fig. 8.1 as shown here in the right bottom panel.

Through these straightforward thought experiments, we show that the apparent cycles of birth–replication–life–death are simply manifestations of the law of mass action with water serving as a solvent for different molecular species. Thus, we propose that not only did life actually originate in this manner, but it continues

to evolve similarly with different molecular species resulting in different kinds of aggregates of different sizes and quantities driven by the law of mass action.

Having proposed a theory for origin of life and evolution of living systems based on the law of mass action, it becomes important for us to address the question of raw materials for the system. As mentioned earlier, while substantial literature focuses on nucleic acids or proteins or both in form of self catalyzing systems for origin of life, we propose amphiphilic assembly (along with, or later with the addition of, a plethora of chemical reactions) in water as a solvent for origins of life. We propose that abundance of carbon on Earth coupled with high-temperature conditions allowed catenation reactions resulting in chains of carbon being formed (black circles in Fig. 8.4). Formation of carbon chains by condensation reactions resulted in water molecules (grey circles, Fig. 8.4)—this water formed was still in vapour form due to the conditions that were resulting in formation of carbon chains.

Thus, before life originated, Earth's atmosphere was rich in gaseous form of carbon-chained molecules along with water vapour along with other molecules in gas phase. With high water vapour content, and heavier carbon-based molecules (including many amphiphiles with carbon chains) having lower volatility, heating and cooling cycles resulted in the formation of liquid pools of water with populations

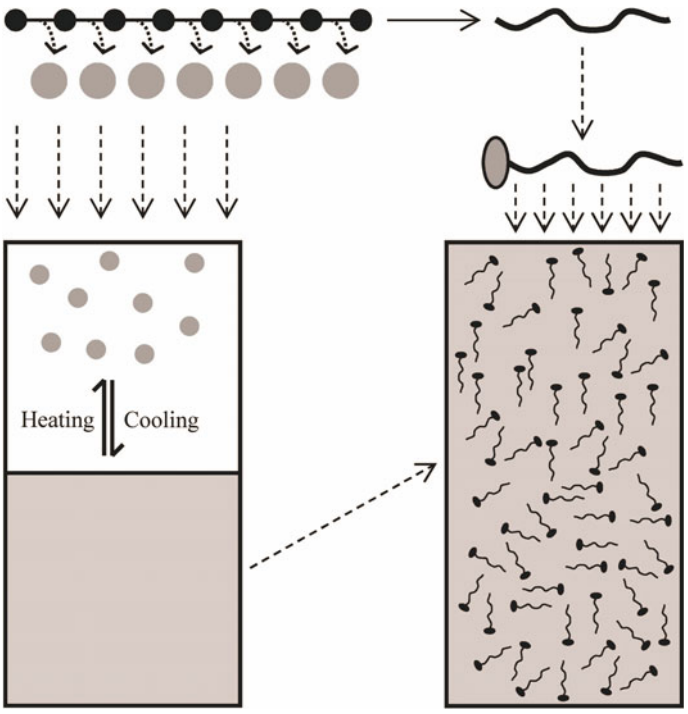

Fig. 8.4 Emergence of conditions for origin of life and evolution—formation of water as a solvent and reaction medium for self-assembling reactions

of amphiphilic molecules. Of course, other chemically reacting systems also must have formed. However, the predominant occurrence of amphiphiles assembling and disassembling in water resulted in the first aggregating systems—these aggregations driven by the energetics of the hydrophobic effect also resulted in what is currently apparent as replication. Simultaneous addition and removal of different molecular species resulted in emergence and sustenance of newer aggregate forms. Here, it is interesting to note that formation of primary polymer chains in living cells, i.e. of nucleic acids and proteins, actually consume water—in test-tube chemistry, polymerization reactions actually result in release of water. Now in the actual intracellular conditions, polymerization reactions resulting in water as a product to form polymer chains cannot take place in aqueous milieu. The presence of water as a solvent at 55 M (concentration of liquid water) would actually drive the reaction backward by law of mass action thereby inhibiting polymerization and favouring the backward reaction due to excess product (water). Operation of the central dogma in living cells actually consumes water—we calculate the amount of this water consumed in Appendix 1. From an evolutionary perspective, this is a very important discovery—once amphiphilic assembly resulted in apparently replicating structures in excess water, more chemical reactions with different molecular species but still driven by the law of mass action took over towards emergence of living cells in their current avatar. Many of these cellular chemical reactions, and certainly the key ones for living system, involve water as a chemically reacting molecular species and not just as a solvent. Finally, having appreciated the role of water as a chemically re(active) molecular species, and not just as a solvent, we also show how different and reproducible morphologies of micellar aggregates emerge in different aqueous chemical environments; see Fig. 8.5 and Appendix 2.

Concluding, we propose that origin of life and evolution of living systems are essentially a result of both the kinetics and the thermodynamics of the hydrophobic effect rooted in the law of mass action, with water as a solvent. While this chapter is aimed at a simplistic introduction of a somewhat orthogonal view on the origin of living systems, it is our hope that self-assembly driven primarily by solvent characteristics will emerge as a key driver of hypotheses in understanding living systems.

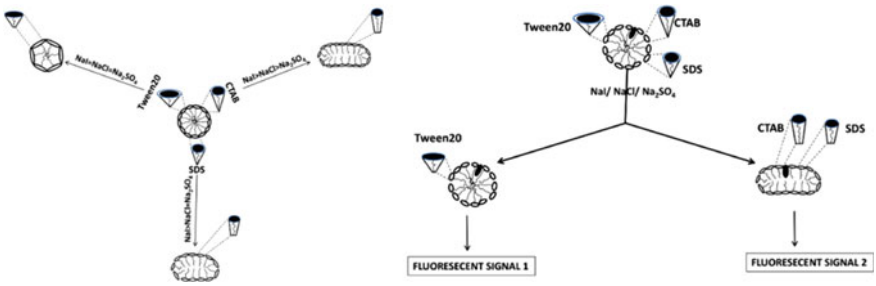

Fig. 8.5 Regulation of amphiphilic self-assembly by water structure and molecular shapes (see Appendix 2 for details)

For this, further studies on the role of the solvent species, both as a reactant and as a reaction medium, will shed further light on origin–sustenance–demise cycles of self-replicating structures as models for origins of life and evolution. Specifically, our proposal emphasizes the importance of amphiphiles and biological membrane-like materials resulting in the first "living" systems rather than nucleic acids and/or proteins. In essence, we are proposing a "micellar world" for origin of life and evolution of living systems rather than a "protein and/or RNA world". One very interesting and appealing aspect of the ideas presented here is that it may not be required to treat understanding of origin of life as a "chicken and egg" problem, if viewed from the perspectives discussed in this work.

Acknowledgements SB is grateful to the Council of Scientific and Industrial Research, Government of India, for research fellowship support. AMC is grateful to IIT Delhi for research fellowship support. AM is grateful to Marie-Hélène Rome and Pierre Pontarotti for their patience.

Author Contributions SB carried out the experimental work for Appendix 2 and co-wrote Appendix 2 with AM, including preparation of figures. AMC carried out literature review and collected the data required for Appendix 1. AM designed the study, formulated the micellar world hypothesis and Life of Micelle Systems thought experiment and wrote the manuscript.

Appendix 1: Water Consumption in Intracellular Central Dogma Operations

Summary Carbon-based chemical polymerization releases water molecules. In contrast, intracellular biopolymerization actually consumes water. Surprisingly, water requirements for intracellular synthesis of proteins and nucleic acids are not accounted for in literature. In this work, we derive the first quantitative expression for the number of water molecules consumed per molecule of protein produced by transcription and translation in a cell. Extrapolating our findings to multi-cellular organisms, we find that a staggering ~90 million litres of water per day is utilized by the current human population only for synthesizing intracellular proteins for survival without replication/reproduction—and this is an underestimate.

Introduction Water as a solvent is assumed to be a prerequisite for life. Not only does water serve as a solvent for chemical reactions inside and outside living cells, but it also serves as a solvent that drives physical (and often non-chemical) self-assembly of amphipathic molecules via the "exclusion by water" principle formally referred to as the hydrophobic effect (Tanford 1973; Silverstein et al. 1998; Southall et al. 2002; Dill et al. 2005; Xu and Dill 2005; Mittal and Grover 2010; Dill and Bromberg 2011). In fact, elucidation of unique properties of water as a solvent for life has been of constant interest (Truskett and Dill 2003; Urbic et al. 2007; Fennell et al. 2010; Mittal and Jayaram 2011; Urbic and Dill 2017; Brini et al. 2017; Urbic and Dill 2018). While appreciating the role of water as a solvent for physical, chemical and physico-chemical interactions governing living systems, it is also pertinent

to consider its role as a chemical reactant in living systems. For example, purely chemically driven polymerization reactions involving formation of carbon-based chains involve release of a water molecule per bond formed. Thus, in such systems, the presence of water as a solvent would not allow a forward reaction resulting in release of water in order to form a bond for extending the polymer due to the high concentration (55.5 M) of surrounding water. However, interestingly in living cells, polymerization of nucleotides resulting in the formation of DNA and mRNA molecules as well as synthesis of polypeptide chains (resulting in proteins) actually utilize water as a reactant for bond formation required for polymer elongation. Surprisingly, this water requirement during the creation of biosynthetic machinery in living cells is largely ignored and not accounted for in the literature, including textbooks on life and cell biology. The apparent assumption of the constitutively present biosynthetic machinery from the perspective of requirements of water as a reactant is in complete contrast to substantially increasing literature on energy requirements for assembling the same biosynthetic machinery. In fact, energetic considerations in biological systems (e.g. living cells) continue to be addressed regularly with respect to cell size and growth (Dill et al. 2011; Naresh et al. 2012; Maitra and Dill 2015; Szenk et al 2017; Wagoner and Dill 2019) along with assembly of, and functional constraints on, proteomes and cell organelles (Ghosh and Dill 2010; Naresh et al. 2010; Ghosh et al. 2016; Santra et al. 2017; Agozzino and Dill 2018). Therefore, in this work, we explicitly address the requirement of water in creation of the biologically synthesized machinery (i.e. proteins). We derive the first-ever formalism for calculating water consumed during the processes of transcription and translation resulting in synthesis of a protein molecule. Our results compel explicit inclusion of water consumed during operation of the central dogma for creation of biosynthetic machinery during considerations of metabolic perspectives on living systems.

Results and Discussion

Accounting for water consumed during transcription and translation First, let us consider transcription. Formation of a phosphodiester bond to extend an mRNA molecule requires one water molecule to hydrolyze the released pyrophosphate (Heinonem 2001; Nelson and Cox 2008). Therefore, addition of each nucleotide to form an mRNA molecule consumes one molecule of water (Heinonem 2001; Nelson and Cox 2008). This implies that synthesis of an mRNA molecule with length = "L_{mRNA}" in terms of number of nucleotides consumes a total of "L_{mRNA} – 1" water molecules (since the number of phosphodiester bonds is one less than the total length due to the 5′ and 3′ termini). Now, each mRNA transcript can be utilized to produce a variable number of protein molecules, generally ranging from 10 to 10,000 (Heinonem 2001; Dill et al. 2011; Lahtvee et al. 2017). Let us assume that the number of protein molecules per mRNA transcript is given by "N_P". Note that each of these protein molecules will have "$L_{mRNA}/3$" residues (since codon size =

3). Therefore, the number of water molecules consumed during transcription for a single protein molecule = "(L_{mRNA} 1)/N_P". The next step is translation. Beyond the presence of an mRNA transcript, translation requires aminoacyl-tRNA molecules. For producing one aminoacyl-tRNA molecule, the first step is activation of an amino acid molecule—this involves hydrolysis of a pyrophosphate by pyrophosphatase which consumes one water molecule (Heinonem 2001; Nelson and Cox 2008; Yang et al. 2009). The activated amino acid, in the form of amino acid-AMP complex, combines with tRNA resulting in a molecule of aminoacyl-tRNA and release of an AMP (Voet et al. 2013). The released AMP is converted into an ADP (Poos et al. 1999). Therefore, formation of a single aminoacyl-tRNA consumes one molecule of water. To extend the polypeptide chain during translation, i.e. for polypeptide elongation, an aminoacyl-tRNA binds with the GTP-bound elongation factor EF-Tu to form a ternary complex. This ternary complex binds to the ribosomal A-site—during this reaction the GTP is hydrolyzed and one water molecule is consumed (for GTP hydrolysis). In addition, polypeptide elongation also involves hydrolysis of EF-G-GTP complex at the ribosomal *P*-site for removal the uncharged tRNA. This hydrolysis consumes one water molecule. Therefore during the incorporation of a single amino acid into an elongating polypeptide chain, starting with formation of aminoacyl-tRNA to the release of uncharged tRNA, three water molecules are consumed. The above is applicable to all amino acids incorporated into an newly forming polypeptide chain except for the first and the last. An initiation complex involving mRNA, 30S ribsome and GTP-fMet-tRNA is formed by hydrolysis of a GTP molecule (thereby consuming one water molecule) for starting translation (Voet et al. 2013). Thus, formation of this initiation complex consumes one water molecule for starting translation (instead of consuming one water molecule for creation of aminoacyl-tRNA). Subsequent steps remain the same—therefore, a total of three water molecules are consumed for starting translation with the first residue. For the last amino acid incorporated in the polypeptide chain, ribosomal hydrolysis of peptidyl-tRNA resulting in the released polypeptide chain along with free tRNA consumes one water molecule (instead of hydrolysis of EF-G-GTP complex at the ribosomal *P*-site for removal the uncharged tRNA). Therefore, three water molecules are consumed for ending elongation with the incorporation of last residue. Summarizing requirements during translation, the total number of water molecules consumed to create a polypeptide chain with total residues = "$L_{mRNA}3$" during translation is "$3 \times L_{mRNA}3$" = "L_{mRNA}. In addition, two water molecules get consumed during termination of translation while releasing the ribosomal subunits and mRNA transcript immediately subsequent to (or simultaneously with) release of the polypeptide chain (Voet et al. 2013). Therefore, the total number of water molecules consumed in the translation step of creating a single polypeptide chain (total residues = "$L_{mRNA}3$") is "L_{mRNA} + 2". Combining transcription and translation, the total water molecules consumed for synthesizing one protein molecule having "$L_{mRNA}/3$" residues = [(L_{mRNA} − 1)/N_P] + [L_{mRNA}+ 2]. Thus,

$$\frac{H_2O \text{ molecules consumed}}{\text{Protein molecule}} = \left(1 + \frac{1}{N_P}\right) L_{mRNA} + \left(2 - \frac{1}{N_P}\right) \tag{8.1}$$

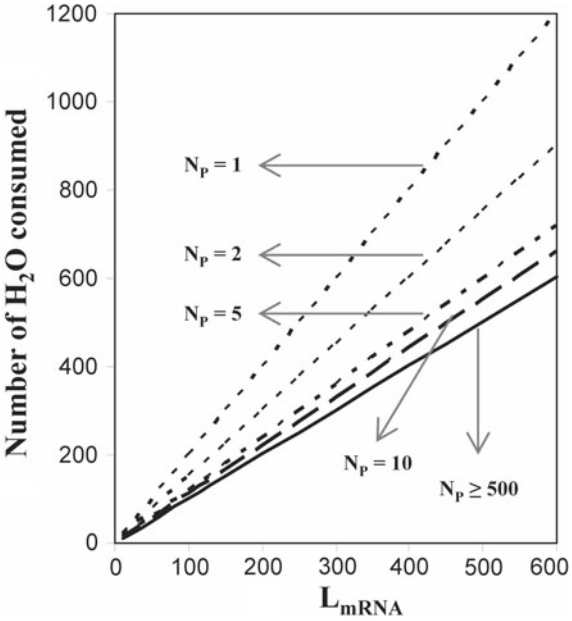

Fig. 8.6 Total number of water molecules consumed for synthesizing (transcription + translation) a protein molecule with "$L_{mRNA}/3$" residues as a function of the length of the mRNA transcript (in terms of number of nucleotides) encoding for the protein molecule. "N_P" is the number of protein molecules synthesized by translating a single mRNA transcript. The plot is based on Eq. (8.1), see text for details

where "L_{mRNA}" is the length of the mRNA molecule for synthesizing a protein molecule with "$L_{mRNA}/3$" residues and "N_P" is the number of protein molecules synthesized per mRNA transcript. Figure 8.6, based on Eq. (8.1) above, shows that beyond "$N_P = 500$", there is negligible change in number of water molecules consumed per molecule of protein synthesized regardless of the size of the protein.

Calculating water consumed only for transcription and translation by a cell Having analytically derived the expression giving water consumption during protein biosynthesis, the next step is to actually apply it to in vivo scenarios. To do so, let us consider *E. coli* cells. The average length of a protein in an *E. coli* cell is 325 residues (Zhang 2000; Dill et al. 2011). Therefore, on an average, $L_{mRNA}/3 = 325 \geq L_{mRNA} = 975$. Assuming $N_P = 50$ (Heinonem 2001; Dill et al. 2011; Lahtvee et al. 2017), the total number of water molecules consumed by an *E. coli* cell for synthesizing one protein molecule $= [\{1 + (1/50)\} \times 975] + [2 - (1/50)] = 996.48$.

An *E. coli* cell has ~3 million protein molecules (15), and a replication time of ~10 min (15). Therefore, the total water consumed by a non-replicating *E. coli* cell for only surviving for 10 min by synthesizing its protein molecules $= 3 \times 10^6 \times 996.48 = 2.98944 \times 10^9$ molecules. Now there are several ways of looking at this interesting result. As an example, let us consider an *E. coli* culture of 10^8 non-replicating cells

per ml—note that is at least an order of magnitude less than a saturated *E. coli* culture (Sezonov et al. 2007). Ten litres of this culture would contain 1×10^{12} cells, and therefore, the total water consumed per day by this culture for only cell survival by protein synthesis would be $(24 \times 60/10) \times 2.98944 \times 10^9 \times 1 \times 10^{12} = 4.3047936 \times 10^{23}$ molecules. This equals (4.3047936/6.023) ~ 0.715 mol of water. One mole of water is 18 ml of liquid water. Therefore, a 10 L culture of non-replicating *E. coli* cells would consume 18 × 0.715 ml ~ 13 ml of liquid water per day only for protein synthesis required for survival. While 13 ml of water per day might appear a small amount, considering simply a stationary batch secondary-metabolite industrial production culture in a reactor of 20 kilolitres (i.e. cells are in pseudo-steady state in stationary phase without replication), it translates to consumption of [(13 ml × 20,000 L)/(10 L)] = 26 L of water by cells only for protein synthesis required for survival. These 26 L of water are not accounted for anywhere in any literature till date. More importantly, since 26 L is ~0.13% of 20 kilolitres, it never gets noticed. As another example, let us extrapolate the results from *E. coli* cells to multi-cellular organisms such as humans. If we consider a human to be equivalent to a trillion (10^{12}) non-replicating E. coli cells, then again, a stagnant human population of ~7 billion would be consuming a staggering $[(13 \text{ ml} \times 7 \times 10^9] = 91$ million litres of water per day just for protein synthesis required for survival without any growth. Of course, this calculation provides an underestimate; however, it strongly highlights the fact that water consumption during transcription and translation needs to be accounted for during our considerations of cell biology and life in general.

Present and future importance of water consumption during intracellular biosynthesis We have derived the first estimates of water consumption during transcription and translation per protein molecule synthesized inside living cells. In modern times, with the availability of whole transcriptome and proteome data especially for different cells growing under different conditions, it would be indeed interesting to calculate the water consumed per "unit functionality" of cells. By knowing the exact number of mRNA transcripts and the number of corresponding protein molecules synthesized specifically during a particular metabolic process of a cell (e.g. glucose metabolism or lipid biosynthesis or even more generalized concept of cell growth), water consumption for creation of biosynthetic machinery required during that specific metabolic process can now be calculated. Our work promises to be a useful tool in planning requirement of water resources for setting up and maintenance of living societies (of both microbial and multi-cellular organisms including humans) on Earth, since water is fast becoming a limiting resource, and even beyond since water requirements will have to be calculated accurately.

Appendix 2: Regulation of Amphiphilic Self-assembly by Water Structure and Molecular Shapes

Summary Structural diversity in lipids maintains the dynamic structure and functions of variably curved membranes in cellular milieu. Distribution of molecular shapes of these lipids drives curvature formation in the membrane structures. In aqueous environment, these amphiphiles are known to form preferred assembled geometries due to the hydrophobic effect. In order to gain insights into the dynamics of individual shapes of amphiphiles accompanying (and possibly leading to) this transition in entire assembled structures, we used tryptophan octyl ester (TOE-probe)-based fluorescence assay on three types of surfactants (anionic, cationic and non-ionic) and alter the structure of water using three different electrolytes. The pKa values, fluorescence and red shift of the TOE incorporated into different micellar structures provide a somewhat direct measure of the role of individual molecular shapes of surfactants resulting in various self-assembled structures in different aqueous environments. Here, we provide evidence that perturbation in water structure alters the individual molecular shape and thus, results in shape transition(s) of micellar structures. However, these changes in molecular shapes are allowed within permissible ranges as dictated by chemical structure of the individual amphipaths. Experimental findings in this work allow an investigation of not only alteration of molecular shapes of individual surfactant molecules in different aqueous environments, but also the role of these alterations in governing the overall structure of the hydrophobic effect-driven macromolecular assemblies.

Introduction Membranes are highly active structures present as plasma membrane and organellar membranes in the cells. Dynamic nature and varied functionality in different membranous compartments are maintained by diversity in their lipid compositions (Van Meer et al. 2008; Andreyev et al. 2010, Bansal and Mittal 2015). In addition to various curvature forming proteins (Zimmerberg and Kozlov 2006; Bansal and Mittal 2013), asymmetric distribution of individual molecular shapes of lipids has been known to induce curvature formation in membranes (McMahon and Gallop 2005). These molecular shapes of amphiphiles have been quantified in terms of "packing or shape parameter" by Israelachvili et al. (1976). There are several reports which support that these shape parameter of membrane lipids dictates the self-assembly of amphiphiles in solvent medium. Experimental evidence showed that change in the membrane composition of RBC with differentially shaped lipid molecules could alter the entire cellular morphology (Christiansson et al. 1985). Membrane remodelling to form differentially curved membranes as required during cellular fission or fusion processes (Chernomordik et al. 1985; Chernomordik and Kozlov 2003), tubules or vesicles formation (Roux et al. 2005; Christian et al. 2009), sorting of lipids and membrane proteins (Mukherjee et al. 1999) and fusion of enveloped virus to host membranes (Chernomordik et al. 1995; Mittal et al. 2002; St Vincent et al. 2010; Zaitseva et al. 2010) have been known to be regulated by the array of various lipids. Few computational studies also reported the coupling between lipid shape and geometry of its assembled structure using bead-based model in molecular

dynamics (MD) simulations (Cooke and Deserno 2006) and shape-based phase separation of lipids using conical linactants segregated at the phase boundary (Schafer and Marrink 2010). Subsequent to development of liposomes as model systems by Bangham (1972), there are very few reports which investigate the mechanism of liposomal assembly (Mittal and Grover 2010). However, micelles have served as a major model system to gain mechanistic insights into the self-assembly process of amphiphiles in aqueous solutions till date. As it is well known that the self-assembly of amphiphiles is driven by the hydrophobic effect in aqueous water (Tanford 1973, 1978), we proposed a testable hypothesis to see the effect of any disturbance created in the structure of liquid water on the molecular shapes of amphipaths and thereby affecting the whole self-assembly process. Water in liquid form is known to be in disordered state having very short range ordered structure as compared to its crystalline state (Tanford 1973). The most accepted model of water structure was given by Eisenberg and Kauzmann (1969) which assumes that water molecules in liquid-state form four hydrogen bonds to their neighbouring water molecules that result a flexible irregular network. Structure of water is known to be affected by the presence of other molecules and electrolytes. Few of the electrolytes have been reported to cause more ordering in the water structures and classified as chaotropes (or water structure breakers) such as NaI and kosmotropes (or water structure makers) such as NaCl, Na_2SO_4 (Nickolov and Miller 2005; Barbosa et al. 2010). Hofmeister series illustrates the order of the effect of these ions on the structure of water (Collins 1997; Marcus 2009; Mahler and Ingmar 2012) and has been extensively studied to explain their effect on the confirmation and stability of proteins (Baldwin 1996; Collins 2004). Kosmotropes, also termed as salting-out salts, are known to decrease the solubility of proteins and cause protein precipitation. Chaotropes are known to increase the solubility of the proteins by increasing their solvent accessible area and termed as salting in salts (Wetlaufer et al. 1964; Zhang and Cremer 2006). Few reports also studied the effect of these electrolytes on micellar systems. Addition of electrolytes has shown to decrease the critical micellar concentration (CMC) of various surfactants indicating their transition from spherical to rod shaped micellar assemblies (Ray and Nemethy 1971; Ericsson et al. 2004). These shape transition in micelles have been indirectly visualized using environment-sensitive fluorescence assays (Rawat and Chattopadhyay 1999; Arora-Sharawat and Chattopadhyay 2007; Chaudhuri et al. 2009, 2012). In addition to this, there are few negative stain EM reports that directly visualized the transition in pure and mixed spherical micelles to flexible rods on presence of salts (Imae et al. 1985; Chakraborty and Sarkar 2004). Few MD simulation studies have also been reported the transition in spherical to cylindrical SDS micelles under the effect of various salts (Sammalkorpi et al. 2009). In spite of several theoretical, computational and experimental studies on the shape transitions in self-assembled structure of amphiphiles or micelles on adding salts, there is no single report available till date that investigates how individual molecular shape of amphiphiles get affected during, or result in, this change in their macromolecular geometry. Thus here, we used three surfactants as per the classification of detergents as anionic (SDS), cationic (CTAB) and non-ionic (Tween20), to study the dynamics of individual molecular shapes of surfactants on altering the water

structure by adding three sodium salts (NaI, NaCl and Na_2SO_4). These electrolytes were known to affect the bulk water properties or ordering of water as NaI < NaCl < Na_2SO_4 (Nickolov and Miller 2005; Barbosa et al. 2010). Using tryptophan octyl ester (TOE as probe)-based fluorescence assay (Arora-Sharawat and Chattopadhyay 2007), we provide evidence that shape of individual amphiphile is a key determinant which regulates the transition in the shape of micelles. Here, we propose that water structure is the most important factor compared to the ionic strength of salt and dielectric constant of solutions which alters the individual shape of amphiphiles leading to change in the shape of the micellar assembly. Based on the above, we are also able to predict the altered molecular shapes of surfactants as well as the shapes of their micellar geometry in absence and presence of these salts.

Materials and Methods SDS, CTAB, Tween-20, NaCl, NaI, Na_2SO_4 and all buffers components were purchased from Sigma-Aldrich Chemicals Pvt. Ltd. TOE was purchased from Santa Cruz Biotechnology, Inc. Milli-Q water was used throughout to prepare each solution.

TOE-based fluorescence assay was performed as given in (Arora-Sharawat and Chattopadhyay 2007) and further optimized for CTAB and Tween-20. Micelles were prepared by dissolving these detergents at higher concentration than their CMC, to ensure the formation of micellar assemblies in their respective solutions. For this, we used 16 mM SDS (CMC 8 mM) (Arora-Sharawat and Chattopadhyay 2007), 8 mM CTAB (CMC 1 mM) (Neugebauer 1990) and 0.5 mM Tween-20 (CMC 0.06 mM) (Helenius et al. 1979). For REES experiments, SDS was used at 48 mM, CTAB at 8 mM and Tween-20 at 16 mM. NaCl, NaI and Na_2SO_4 were used in 0.5 M concentration for SDS and CTAB and 1.5 M for Tween-20. The maximum molar ratio of TOE/SDS was 1:120 (mol/mol), for TOE/CTAB 1:120 (mol/mol) and for TOE/Tween-20 1:40 (mol/mol). Stock solution of TOE was dispensed to get the optimized probe to detergent ratio in each tube and dried under nitrogen purge while keeping them at ~35 °C. Then the probe was further lyophilized for ~3 h. We added desired volume of detergent and salt (to get the desired final concentration) in the dried probe and vortexed this mixture for ~3 min. The buffers used were at 5 mM; KCl-HCl (pH 1 and 2), acetate (pH 4 and 5), phosphate (pH 6), MOPS (pH 6 and 7), Tris (pH 8 and 9), CAPS (pH 10–12), Na_2HPO_4 (pH 11.5 and 12). Blanks were prepared without TOE and controls were prepared without detergents. All samples were equilibrated at ~28 °C in the dark for 1 h. Fluorescent measurements were performed on Cary Eclipse fluorescence spectrophotometer (Agilent Technologies) using Quartz cuvette of 1 cm path length. Slit width used in all experiments was 2.5 mm except for REES and Tween-20 experiments where 5-mm-slit width was used in order to get the optimized signals. Sigmoid and Peak fittings were performed to get $r2 > 0.9$ using OriginPro8. Sigmoid fitting was done using dose–response function as shown below:

$$y = A1 + \frac{A2 - A1}{1 + 10^{(\log x0 - x)P}};$$

where $A2$ is y max, $A1$ is y min and P is hill slope.

Now, for $[HA] \overset{K}{\Leftrightarrow} [H^+] + [A^-]$

Henderson–Hasselbalch equation: $pH = pKa + \log\left(\frac{[A-]}{[HA]}\right)$

Here, $[A-] = (y\text{max} - y)$ and $[HA] = (y - y\text{min})$

So,

$$
\begin{aligned}
& pH = pKa + \log\left[\frac{(y\text{max} - y)}{(y - y\text{min})}\right] \\
& \Rightarrow pH - pKa = \log\left[\frac{(y\text{max} - y)}{(y - y\text{min})}\right] \\
& \Rightarrow 10^{(pH-pKa)} = \frac{y\text{max} - y}{y - y\text{min}} \\
& \Rightarrow 10^{(pH-pKa)} = \frac{y\text{max} - y\text{min} + y\text{min} - y}{y - y\text{min}} \\
& \Rightarrow y10^{(pH-pKa)} - y\text{min}10^{(pH-pKa)} = y\text{max} - y\text{min} + y\text{min} - y \\
& \Rightarrow y10^{(pH-pKa)} + y = y\text{min}10^{(pH-pKa)} + y\text{min} + (y\text{max} - y\text{min}) \\
& \Rightarrow y\left[1 + 10^{(pH-pKa)}\right] = y\text{min}[1 + 10^{(pH-pKa)}] + (y\text{max} - y\text{min}) \\
& \Rightarrow y = \frac{y\text{min}\left[1 + 10^{(pH-pKa)}\right] + (y\text{max} - y\text{min})}{\left[1 + 10^{(pH-pKa)}\right]} \\
& \Rightarrow y = y\text{min} + \frac{(y\text{max} - y\text{min})}{1 + 10^{(pH-pKa)}} \\
& \Rightarrow y = A1 + \frac{(A2 - A1)}{1 + 10^{(pH-pka)}}
\end{aligned}
$$

Peak fitting was done using extreme function as given below:

$$y = y0 + A\mathrm{e}^{(-\mathrm{e}^{(-z)}-z+1)}; \quad z = \frac{(x - xc)}{w};$$

where, w is width of the curve, xc is the value at x-axis for $y = y\text{max}$ and A is amplitude of curve.

Results and Discussion

TOE fluorescence as an indicator of shape transition in micelles We first incorporated TOE in SDS micelles and monitored its fluorescence at different pH values. From the sigmoidal data obtained from pH 5 to 12 (due to the protonation and deprotonation the TOE amino group), we found pKa values of 10.1 in the absence of any salt and 8.9 (using same buffers as used in Arora-Sharawat and Chattopadhyay 2007)

and 9.1 (using different buffers at pH 6, 11.5 and 12) in presence of 0.5 M NaCl (see Fig. 8.7).

The difference of 1.2 and 1.0 unit, respectively, in pKa values was similar to the difference in pKa values reported earlier for TOE incorporated into SDS micelles under different environments. This difference is observed due to different nature of incorporation of TOE into spherical- and rod-shaped micelles—as TOE is known

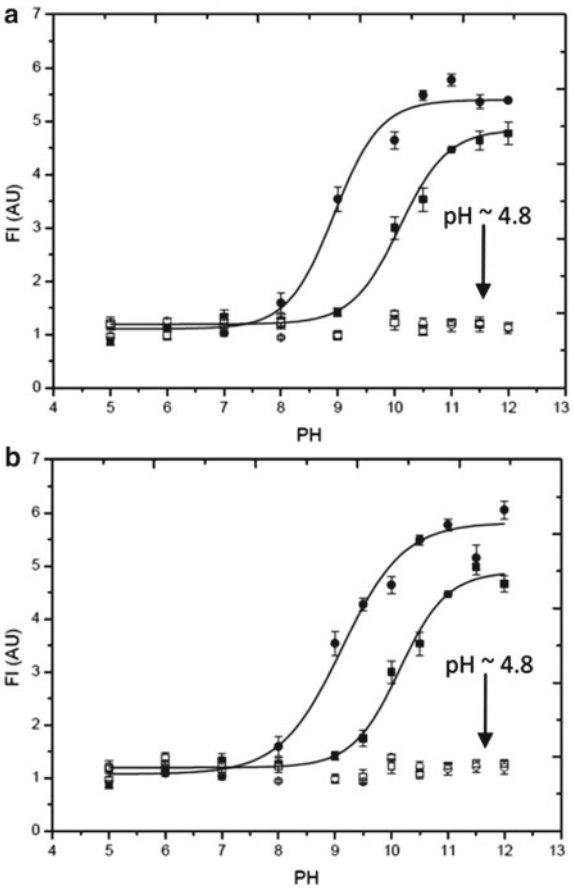

Fig. 8.7 TOE fluorescence in spherical- and rod-shaped SDS micelles. **a**, **b** represent mean ± SE of fluorescence intensity of TOE in SDS micelles in the absence (filled squares) and presence (filled circles) of 0.5 M NaCl as a function of pH. In panel (**a**), buffers used in Arora-Sharawat and Chattopadhyay (2007). In panel (**b**), different buffers were used at pH 6, 11.5 and 12. The excitation wavelength was 280 nm, and emission was recorded at 340 nm. TOE/SDS ratio was 1:800 (mol/mol). The pH of all samples was lowered to 4.8 ± 0.1 using 1 M acetic acid and fluorescence was shown as (empty squares) in the absence and (empty circles) presence of 0.5 M NaCl

to give environment-sensitive fluorescence signals (Arora-Sharawat and Chattopadhyay 2007). We further extended the work to test whether addition of two different salts like NaI and Na_2SO_4 will also affect the pKa in similar way as NaCl. The primary objective was to explore how different liquid water structure, affected by salts/ions in the order Na_2SO_4 > NaCl > NaI or SO_4^{2-} > Cl^- > I^- (Nickolov and Miller 2005; Barbosa et al. 2010) with I-being the most disruptive (known to cause most disorderness in liquid water structure), could impact individual shape parameters of SDS (due to different hydration shell sizes around the head groups of individual molecules) thereby affecting overall geometry of the micellar self-assembly. Interestingly, we found that SDS micelles show a pKa of 9.1 with 0.5 M Na_2SO_4 (similar to NaCl) and 8.7 with 0.5 M NaI (Fig. 8.8).

Therefore, in terms of micellar assembly, the order was found with SDS micelles as NaI > NaCl = Na_2SO_4. This indicates that effect of anions or salts on water structure is also playing a role in the sphere- to rod-shaped transition of SDS micelles in addition to the shielding effect of Na+ which helps in minimizing the interfacial area of SDS molecules and induces tighter and closer packing. To further understand the role of water structure on the shapes of micelles, we monitored the change in fluorescence intensity of TOE bound to CTAB micelles (CTAB is a positively charged detergent). Electron microscopy reports have suggested that CTAB aggregates to form large flexible rods of 2.2–3.0 nm radius in presence of 0.5 M NaBr (Imae et al. 1985). Thus, we treated CTAB micelles with the same concentration (0.5 M) of each salt to see their effect on its assembly process. Here, we observed a pKa of 7.3 in spherical micelles or in absence of any salt and pKa of 5.6 in 0.5 M NaCl and 6.0 in 0.5 M Na2SO4 (see Fig. 8.8). Thus, we found the difference of 1.7 units in addition of NaCl and 1.3 units in Na_2SO_4. Interestingly, we could not take the fluorescence readings after addition of 0.5 M NaI to CTAB as this solution becomes turbid and milky white in appearance—indicating macromolecular assemblies much larger than micelles, e.g. possible long hexagonal phases or some other larger structures resulting high colloidal and turbid content. Results with CTAB indicate the order as NaI > NaCl > Na_2SO_4 which is in reverse to the charge density of these anions. It is interesting to note that this order is similar (but not the same) to that obtained with SDS. Therefore, in spite of the detergents being negatively (SDS) or positively charged (CTAB), similar order of effect of anions on micellar assembly clearly suggests that shape transition in micellar assembly is majorly the consequence of perturbance in the structure of water which obviously affects the overall shape of individual surfactant molecules. A larger hydration volume of the surfactant will lead to a larger head to tail ratio, resulting in more conical individual molecular shapes which self-assembled into spherical micelles. Subsequently with decreasing head size, individual molecular shapes start becoming cylindrical leading to cylindrical micellar assemblies. Having obtained interesting insights by using negatively and positively charged detergents, we further investigated the (possible) shape transitions in non-ionic detergent, Tween-20. It is known that only high concentrations of salts may affect the CMC and/or the assembly of non-ionic detergents (Ray and Nemethy 1971). Thus, we used 1.5 M concentration for each salt as maximum solubility of Na_2SO_4 is 1.5 M at 28 °C. Here, we observed pKa of 7.1 without any salt (spherical micelles) which decreases

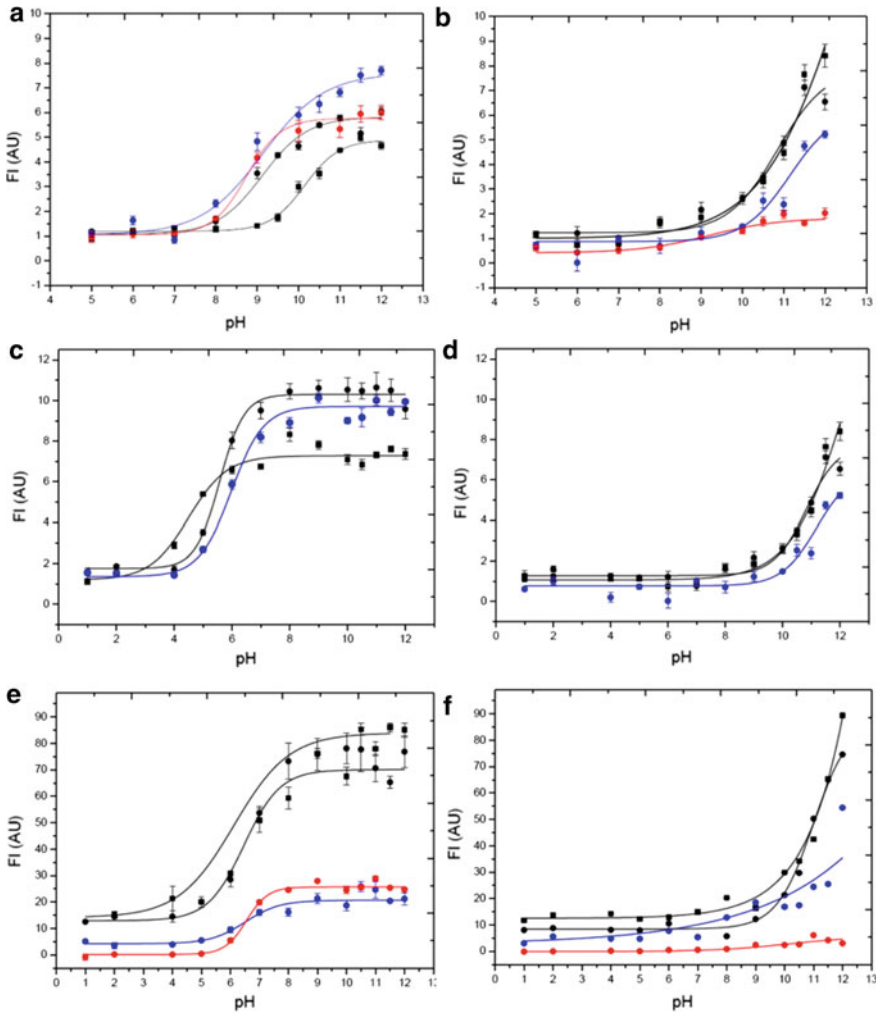

Fig. 8.8 TOE fluorescence in spherical- and rod-shaped micellar assemblies. Panels **a**, **c**, **e** represent mean ± SE of fluorescence intensity of TOE in micelles in the absence (squares) and presence (circles) of salts as a function of pH. Panels **b**, **d**, **f** represent mean ± SE of fluorescence intensity of TOE in controls (without micelles) in the absence (squares) and presence (circles) of salts as a function of pH. Panels **a**, **b** represent SDS micelles, **c**, **d** used for CTAB and **e**, **f** for Tween-20 micelles. Black circles were used for NaCl, blue circles for Na_2SO_4 and red circles were used for NaI. The excitation wavelength was 280 nm, and emission was recorded at 340 nm. TOE/SDS ratio was 1:800, TOE/CTAB ratio was 1:400 and TOE/Tween-20 was 1:80 (mol/mol)

to 6.5 in case of each of the three salts (Fig. 8.8). Remarkably, we observed similar pKa and a difference of 0.6 units in case of all three salts. So, the order found here is NaI = NaCl = Na_2SO_4. Here, it is important to note that as compared to the SDS and CTAB, Tween-20 contains a large bulky head group to being with. Clearly, this large head group seems to limit the effect of salts since the changes in hydration volume of the head group (due to changed water structure) are negligible compared to original head size. Therefore, the individual molecular shape of Tween-20 remains same in all three salts as conical resulting in only spherical micelles. Therefore, our results clearly show that transition in the molecular shapes of amphiphiles is the root cause of the shape transitions in micellar assembly. However, this change in shape parameter is allowed within the constraints of its chemical structure and in turn facilitated by the variation in water structure in aqueous medium.

Red edge excitation shift of TOE in spherical and cylindrical micelles Red edge excitation shift (REES) is defined as the shift of emission spectra towards longer wavelength on increasing the excitation wavelength. This effect would be seen if fluorophores occupy motionally confined regions such as interfacial regions of micelles as occupied by TOE (Arora-Sharawat and Chattopadhyay 2007). Thus, REES measurements on TOE would also provide an assay to monitor the transition of micellar geometries. Therefore, in order to confirm our above findings based on pKa values, we performed REES experiments on SDS, CTAB and Tween20 micelles. In case of SDS, REES experiments were conducted at pH 5 and 11 only as TOE predominately presents in protonated form at pH 5 and deprotonated forms exist at pH 11. Similarly, for CTAB, REES experiments were performed at pH 2 and pH 11. In case of Tween-20, pH 4 and pH 11 were used for REES experiments (Fig. 8.8). We observed a red shift of 12 nm (336 ± 0.03 nm to 348 ± 0.09 nm) in the maximum fluorescence emission of TOE in SDS micelles with increasing pH from 5 to 11 due to the deprotonation of TOE. As expected, we also observed a similar blue shift of ~2 nm (336 nm to 334) in fluorescence emission maxima at pH 5 and from 348 nm to 346 nm at pH 11 upon addition of 0.5 M NaCl (see comparative Table 8.1).

These results indicate that the shape transition of the micelles was accompanied by the decrease in polarity around TOE (Arora-Sharawat and Chattopadhyay 2007). Interestingly, we observed similar blue shift with all three salts. Figure 8.9 shows fluorescence emission spectra of TOE in SDS micelles at pH 5 and pH 11 in absence and presence of 0.5 M NaCl, Na_2SO_4 and NaI.

We observed a shift in emission maximum from 336 to 341 nm and REES of 5 nm at pH 5 in spherical micelles (Fig. 8.10).

We also observed 348–351 nm shift and REES of 3 nm at pH 11 in spherical micelles. After adding 0.5 M NaCl, we found 334–340 nm shift and REES of 6 nm at pH 5 and 346–350 nm shift with REES of 4 nm at pH 11 in rod-shaped SDS micelles. A comparative Table 8.2 was inserted to compare our observation with the previously reported work. Again with 0.5 M Na_2SO_4, emission shift was found from 334 to 340 nm, i.e. REES of 6 nm at pH 5 and 346–350 nm with REES of 4 nm at pH 11. We observed highest shift from 334 to 342 nm, i.e. REES of 8 nm

Table 8.1 Fluorescence emission maximum of TOE in SDS, CTAB and Tween-20 micelles at 280 nm

Host	Fluorescence emission maximum from Arora-Sharawat and Chattopadhyay (2007) (nm)	Fluorescence emission maximum from this work (nm) [mean ± SE]
(A) pH 5		
SDS micelles	335	336 ± 0.03
SDS micelles (in presence of 0.5 M NaCl)	332	334 ± 0.1
SDS micelles (in presence of 0.5 M Na_2SO_4)	NA	334 ± 0.07
SDS micelles (in presence of 0.5 M NaI)	NA	334 ± 0.3
(B) pH 11		
SDS micelles	345	348 ± 0.09
SDS micelles (in presence of 0.5 M NaCl)	343	346 ± 0.09
SDS micelles (in presence of 0.5 M Na_2SO_4)	NA	346
SDS micelles (in presence of 0.5 M NaI)	NA	346 ± 0.1
(A) pH 2		
CTAB micelles	NA	339 ± 0.06
CTAB micelles (in presence of 0.5 M NaCl)	NA	337 ± 0.08
CTAB micelles (in presence of 0.5 M Na_2SO_4)	NA	339 ± 0.1
(B) pH 11		
CTAB micelles	NA	351 ± 0.66
CTAB micelles (in presence of 0.5 M NaCl)	NA	345 ± 0.13
CTAB micelles (in presence of 0.5 M Na_2SO_4)	NA	347 ± 0.04
(A) pH 4		
Tween-20 micelles	NA	335
Tween-20 micelles (in presence of 1.5 M NaCl)	NA	339
(A) pH 11		
Tween-20 micelles	NA	342 ± 0.03
Tween-20 micelles (in presence of 1.5 M NaCl)	NA	342 ± 0.03

NA stands for not available

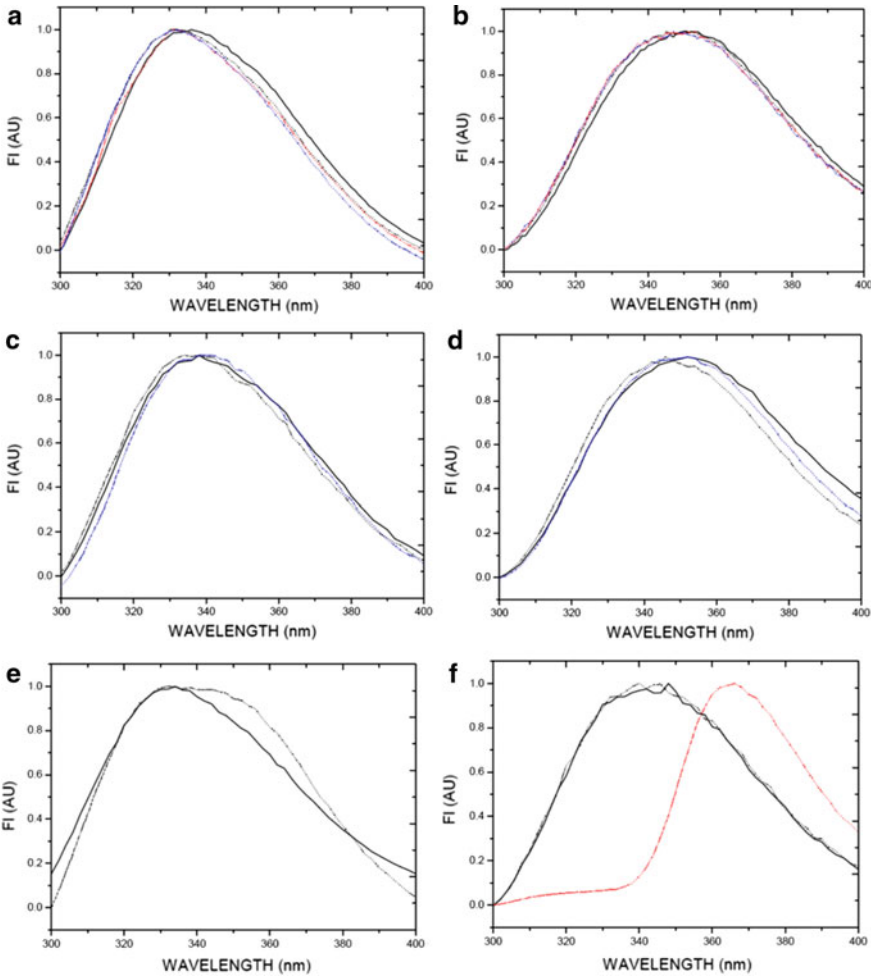

Fig. 8.9 Fluorescence emission spectra of TOE in micelles. Panels **a**–**f** represent emission spectra of TOE bound to micelles in the absence (solid line) and presence (dotted line) of salts. Panels **a**, **b** were used for SDS micelles at pH 5 and pH 11, respectively. Panels **c**, **d** represent emission spectra of TOE bound to CTAB micelles at pH 2 and 11, respectively. Panels **e**, **f** represent Tween-20 micelles at pH 4 and 11, respectively. Black colour was used for NaCl, blue for Na_2SO_4 and red was used for NaI. The excitation wavelength was 280 nm. TOE/SDS ratio was 1:120 at pH 5 and 1:160 at pH 11. TOE/CTAB ratio was 1:120 at pH 5 and 1:160 at pH 11. TOE/Tween-20 ratio was 1:40 at pH 4 and 1:60 (mol/mol) at pH 11

at pH 5 and a shift of 346–350 nm with REES 4 nm at pH 11 in 0.5 M NaI or in rod-shaped micelles. The presence of higher REES in case of NaI at pH 5 indicates the formation of most tightly packed rods in present of NaI. Thus, REES experiments also suggest that the effect of ordering on shape transition of SDS micelles, i.e. NaI >

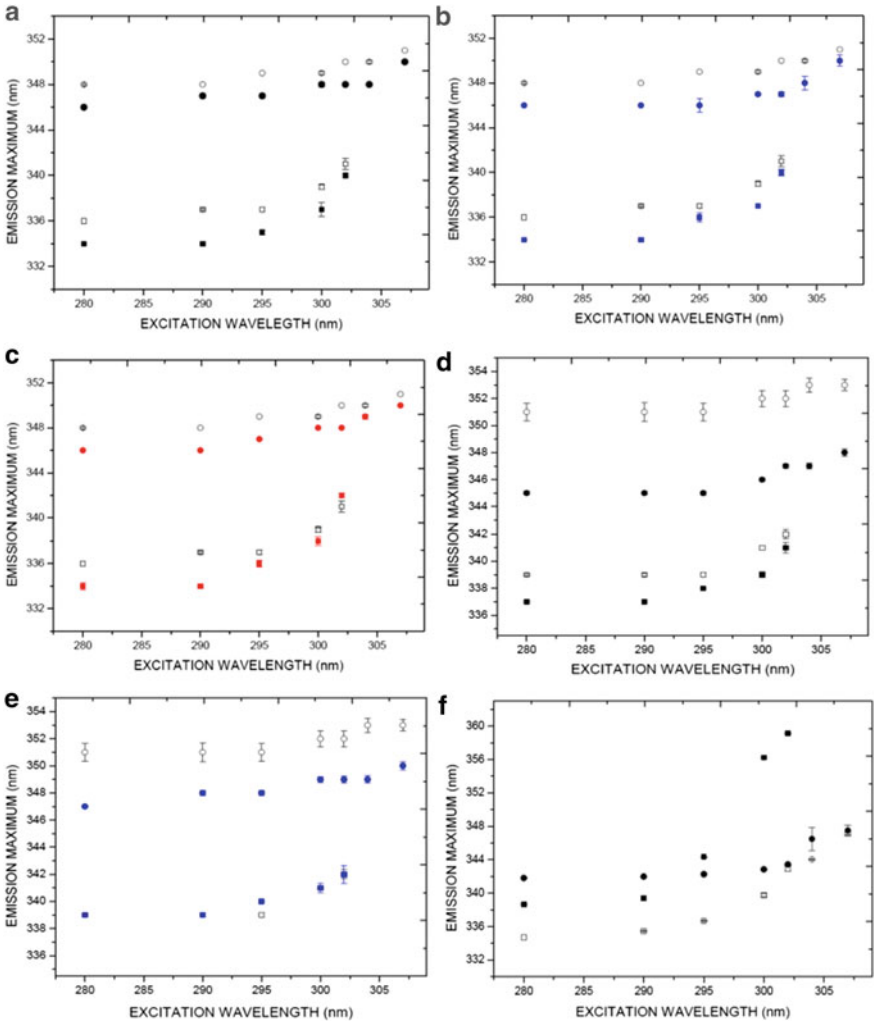

Fig. 8.10 Change in emission maximum on increasing excitation wavelength of TOE in micelles. **a**–**c** represent emission maximum in SDS micelles at pH 5 in the absence (empty squares) and presence (filled squares) of salt, and pH 11 in the absence or spherical micelle (empty circles), the presence of salt or rod-shaped (filled circles) micelles. Panel **d**, **e** represent emission maximum in CTAB micelles at pH 2 and pH 11. Panel **f** represents emission maximum in Tween-20 micelles at pH 4 and pH 11. Black coloured filled symbols represent NaCl, blue colour was used for Na_2SO_4 and red represents NaI. TOE/SDS ratio was 1:120 at pH 5 and 1:160 at pH 11. TOE/CTAB ratio was 1:120 at pH 5 and 1:160 at pH 11. TOE/Tween-20 ratio was 1:40 at pH 4 and 1:60 (mol/mol) at pH 11

Table 8.2 Red edge excitation shift in TOE bound to SDS, CTAB and Tween-20 micelles

Host	REES reported in Arora-Sharawat and Chattopadhyay (2007) (nm)	REES observed from our work (nm)
(A) pH 5		
SDS micelles	4	5
SDS micelles (in presence of 0.5 M NaCl)	6	6
SDS micelles (in presence of 0.5 M Na_2SO_4)	NA	6
SDS micelles (in presence of 0.5 M NaI)	NA	8
(B) pH 11		
SDS micelles	4	3
SDS micelles (in presence of 0.5 M NaCl)	5	4
SDS micelles (in presence of 0.5 M Na_2SO_4)	NA	4
SDS micelles (in presence of 0.5 M NaI)	NA	4
(A) pH 2		
CTAB micelles	NA	3
CTAB micelles (in presence of 0.5 M NaCl)	NA	4
CTAB micelles (in presence of 0.5 M Na_2SO_4)	NA	3
(B) pH 11		
CTAB micelles	NA	2
CTAB micelles (in presence of 0.5 M NaCl)	NA	3
CTAB micelles (in presence of 0.5 M Na_2SO_4)	NA	3
(A) pH 4		
Tween-20 micelles	NA	8
Tween-20 micelles (in presence of 0.5 M NaCl)	NA	20
(B) pH 11		
Tween-20 micelles	NA	5
Tween-20 micelles (in presence of 0.5 M NaCl)	NA	5

NA stands for not available

NaCl = Na_2SO_4, as suggested by the difference in pKa values of TOE fluorescence in micellar assemblies.

Figure 8.9 depicts fluorescence spectra of CTAB bound TOE at pH 2 and 11 in absence and presence of 0.5 M NaCl, and Na_2SO_4. We observed a red shift of 12 nm in the maximum fluorescence emission of TOE in CTAB micelles (from 339 to 351 nm) upon increasing the pH from 2 to 11 due to the deprotonation of TOE (see Table 8.1). We observed a blue shift of 2-6 nm in the maximum of fluorescence emission (from 339 to 337 nm, and 351 to 345 nm) upon addition of 0.5 M NaCl at both pH which indicates decrease in polarity around micelle bound TOE due to the sphere- to rod-shaped transition of the CTAB micelles (see Table 8.1). We observed a blue shift of 4 nm in the maximum of fluorescence emission (from 351 to 347 nm) upon addition of 0.5 M Na_2SO_4 at pH11. However at pH 2, no blue shift was observed in case of Na_2SO_4. We observed 339 to 342 nm shift in emission maximum and REES of 3 nm at pH 2 in spherical micelles (see Fig. 8.10 and Table 8.2). At pH 11, a shift from 351 to 353 nm was found with REES of 2 nm in spherical micelles. We found 337to 341 nm shift and REES of 4 nm at pH 2 in 0.5 M NaCl or in rod-shaped micelles. We observed 345–348 nm shift and REES of 3 nm at pH 11 in 0.5 M NaCl or in rod-shaped micelles. In case of 0.5 M Na_2SO_4, we observed 339–342 nm shift, i.e. REES of 3 nm at pH 2, and 347–350 nm shift with REES of 3 nm at pH 11. Thus, we found increased REES in case of NaCl as compared to Na_2SO_4 which indicates tighter packing of surfactants in presence of NaCl than Na_2SO_4. We could not perform REES experiments on NaI because of the formation of insoluble particles in milky white solution. Thus, REES values also suggest that the effect of ordering on shape transition of CTAB micelles is NaI > NaCl > Na_2SO_4.

Figure 8.8 represents fluorescence emission spectra of TOE in Tween-20 micelles at pH 4 and pH 11 in absence and presence of 1.5 M NaCl and NaI. We observed a red shift of 7 nm in the maximum fluorescence emission of TOE in Tween-20 micelles (from 335 to 342 nm) upon increasing the pH from 4 to 11, indicative of deprotonation of TOE (Table 8.1). There was no blue shift observed in addition of 1.5 M NaCl, and we could not capture these signals in case of 1.5 M NaI and Na_2SO_4 also. Thus, REES experiments did not provide any insights into Tween-20 micellar assembly in different salts. That said, it can also be interpreted that Tween-20 micellar assembly is not, or equally affected, by different salts—a result that is in agreement with our earlier findings using pKa values.

Predicted possible molecular and assembled micellar shapes of surfactants

Above observations clearly support that the shape transition from spherical to cylindrical micelles is largely govern by the molecular shape of surfactants under the effect of altered water structures. Extent to which these molecular shapes can change seems to be dependent upon the degree of perturbation in the structure of liquid water. More compact rods were observed in case of salt causing less ordering in water structure. However, chemical structure of each amphiphiles itself creates some constraints up to which maximum transition in these molecular shapes are permissible. Here based

on these inferences, we predict the possible change in molecular shapes and assembled micellar structure in the absence and presence of three different electrolytes (Fig. 8.11).

Israelachvili et al. (1976) gave a concept of shape parameter which defines the individual shapes of the amphipathic lipid molecules as $S = v/al$, where "v" represents hydrophobic tail volume of the lipid, "a" is the optimum interfacial head area and l is the maximum tail length of the amphiphiles. It was also proposed that this packing parameter or shape parameter can determine the phase of different lipids such as for $S < 1/3$ will form spherical micelles, $1/3 < S > 1/2$ will form non-spherical micelles, $1/2 < S > 1$ form bilayers and $S > 1$ will form inverted structures. Tanford (1973) and (1978) also proposed geometrical considerations and theoretical equations to compute for the maximum extended length of the lipid and core volume of spherical micelles or hydrophobic volume of individual lipid from their chemical structures as:

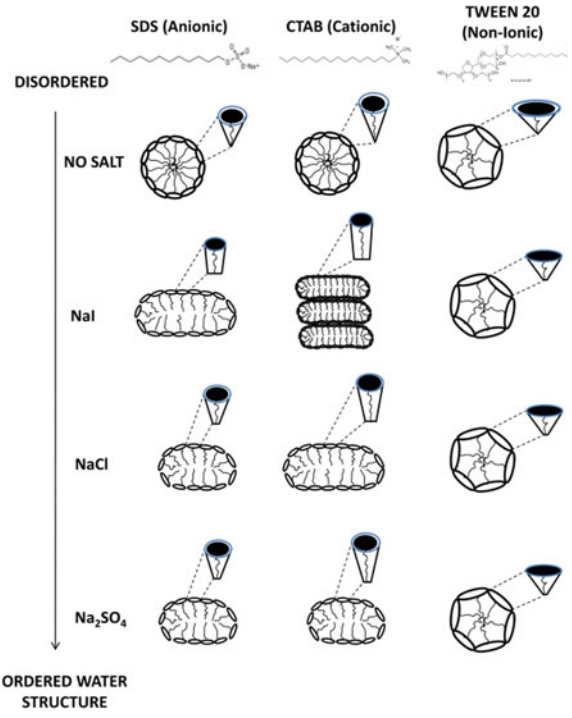

Fig. 8.11 Predicted possible shapes of individual surfactants and micellar assemblies. Figure illustrates the possible coupling between the effect of electrolytes on water structures and shape transition in micellar assembly. NaI, which tends to induce more disordering as compared to NaCl and Na_2SO_4, causes maximum reduction in the hydrodynamic radius around the interfacial head region of SDS and CTAB. This further induces more cylindrical geometry and thus leads to the formation of longer rods in presence of NaI. However, this effect was completely absent in Tween-20 due to the steric hindrance produced by its bulky head group

$\boldsymbol{l = 1.5 + 1.265\, n'c}$, where l is the extended length of the hydrophobic tail in Å and $n'c$ is the number of embedded carbons in the core of micelle.

$\boldsymbol{v = \left(27.4 + 26.9\, n'c\right)m'}$, where v is the core volume of micelle in $(Å)^3$, $n'c$ is the number of embedded carbons in the core of micelle and m' is the number of hydrocarbon chain per micelle (or equal to aggregation number in single-tailed surfactants). However, "a" is interfacial area between head and tail region and depends on the physico-chemical conditions. We used these equations and computed the volume and length for spherical micelles of SDS, CTAB and Tween-20 on the basis of their chemical structures and other available information. SDS and CTAB have minor differences in their extended lengths (16.7 Å and 21.7 Å, respectively) and hydrophobic tail volumes (350.2 $Å^3$ and 457.8 $Å^3$, respectively) and thus should have similar S-values which are also indicated from their similar aggregation numbers ~62 (Arora-Sharawat and Chattopadhyay 2007) and ~60 (Neugebauer 1990), respectively. On the other hand, Tween-20 consists of a large bulky head group and tail length of 12 carbons (tail length is similar to SDS i.e. 16.7 Å). Therefore, Tween-20 has high interfacial surface area which results into a wide-shaped cone geometry that cannot be accommodated in large numbers to form spherical micelles with aggregation number ~22 (Acharya et al. 1997). Addition of electrolytes in all three detergents decrease the interfacial surface area of each molecule which facilitate the change in individual molecular shape from conical to upright truncated cone and thus, further results cylindrical micelles. However, permissible range up to which change in individual molecular shape is possible, actually conferred by its own chemical structure or geometrical constraints under the influence of hydrophobic effect. It is known that these salts affect the structure of water as Na_2SO_4 > NaCl > NaI (Nickolov and Miller 2005; Barbosa et al. 2010). In case of charged micelles (SDS and CTAB), NaI shows its maximum effect in allowing the formation of long compact cylindrical rods and even form much bigger particles showing hexagonal phase formation in case of CTAB. This indicates that NaI induces maximum reduction in the interfacial surface area of individual surfactant and thus aids maximum transition in their molecular shapes to form almost cylindrical-shaped molecules, which in turn, favour the formation of long compact rods. However, this effect is absent in case of non-ionic detergent (Tween-20) because of its substantially bulkier head group which limits the decrease in its effective surface area and thus, predominantly conical individual molecules result in formation of spherical micelles in presence of any salt. Additionally, shape transition in micelles known to be closely coupled with the drastic decrease in CMC of micelles on addition of electrolytes (Ray and Nemethy 1971; Imae et al. 1985; Rawat and Chattopadhyay 1999; Chakraborty and Sarkar 2004; Ericsson et al. 2004; Arora-Sharawat and Chattopadhyay 2007; Chaudhuri et al. 2009, 2012). For example; CMC of SDS (anionic) is 8.0 mM which drops to 0.5 mM in presence of 0.5 M NaCl (Tanford 1973). However, non-ionic surfactants (usually have bulky head group which provide lot of steric hindrance) require high concentration of salts as compared to charged surfactants to cause significant changes in their CMC and/or formation of cylindrical micelles (Ray and Nemethy 1971). Conceptually, shape parameter is also defined as a post-assembly parameter; i.e. shape parameter can be computed only after the formation of an assembled geometry. Our study reports

an increase in the *S* value of surfactants (due to decrease in the interfacial area of surfactants in the presence of salts) accompanied their transition from globular to rod-shaped micelles. Thus, CMC and shape parameter (*S*) seem to share an inverse relationship and act as two indicators to monitor the change in micellar geometry. Our findings clearly provide evidence that individual molecular shape of amphiphiles that are primarily responsible for different geometries of hydrophobic effect-driven self assemblies, can be altered by changing the structure of water. Interestingly, recent studies reported that the restricted non-random dipolar arrangement of water molecules in cylindrical micelles led to substantial changes in the dipole potential of micelles. Similar to our results, it has been reported that this change does not depend on the charge of surfactants and was absent in non-ionic detergents (Sarkar and Chattopadhyay 2015, 2016). This clearly supports that structure and orientation of water molecules around the amphiphiles play a crucial role in facilitating the transition in their macromolecular assembly. Thus, this work provides a strong direction towards further studies for creating/controlling geometrical aspects of hydrophobic effect-driven macromolecular self-assembled structures by varying water structure.

Conclusions Membrane structures undergo continuous rearrangements or remodelling during various cellular processes. Enormous diversity and distribution of these membrane lipids maintain the curvature and functionalities in various membranous organelles. It has been shown that the asymmetric distribution of individual molecular shapes of lipids could induce curvature formation in membranes. Preference of individual molecular shapes to form a particular phase in aqueous solutions has been investigated using computational, theoretical and experimental approaches. Micelles have served as a widely studied experimental system to understand the self-assembly of amphiphiles driven by hydrophobic effect. Structure of water, that provides the aqueous medium for micellar assemblies, has been known to be altered by addition of electrolytes. While addition of these salts had been reported to induce sphere to cylindrical micelle formation in various surfactants, its impact on individual molecular shapes of the self-assembling surfactants that leads to formation of the final micellar geometry was unclear prior to this work. Thus, in order to study the dynamics of molecular shapes of surfactants accompanying the sphere- to rod-shaped transition in micelles, we used two charged: SDS (anionic), CTAB (cationic) and one non-ionic (Tween-20) detergent. Three electrolytes were used to disturb the water structure by increasing the orderness in liquid water. Inspite of common Na+ ions in all three salts, we observed difference in the pKa values of TOE bound to SDS micelles in case of each salt. This indicates that the hydrophobic effect plays a major role as compared to the shielding effect of Na+ ions on negative charge of SDS. In CTAB bound TOE, we found maximum difference in pKa in NaI (similar to SDS) than NaCl and Na_2SO_4. This suggests that the charge on the micellar assembly is not so critical. However, this is structure of water which drives the modification in the individual molecular shapes that further, act as the key determinant in controlling the self-assembly of micellar structures. This inference was also supported by Tween-20 where all three salts showed equal pKa values because of the large bulky head group of Tween-20. Thus, these findings provide evidence that the molecular shapes provide the first

constraint and act as a primary factor in controlling the self-assembly of amphiphiles. These molecular shapes can be altered by perturbing the water structure; however, more disordering or lesser disturbance in bulk water structure yields more compact long rods (as in case of NaI) as compared to the water with more ordered structures (with NaCl and Na_2SO_4). Based on the above findings, we can now also predict the possible changes in individual molecular shapes of surfactants and thus their impact on the shape of overall assembled micelles in different aqueous conditions.

References

Acharya KR, Bhattacharya SC, Moulik SP (1997) The surfactant concentration-dependent behaviour of safranine T in Tween (20, 40, 60, 80) and Triton X-100 micellar media. J Photochem Photobiol A Chem 109:29–34

Agozzino L, Dill KA (2018) Protein evolution speed depends on its stability and abundance and on chaperone concentrations. Proc Natl Acad Sci USA 115:9092–9097

Andreyev AY, Fahy E, Guan Z, Kelly S, Li X, McDonald JG, Milne S, Myers D, Park H, Ryan A, Thompson BM, Wang E, Zhao Y, Alex Brown H, Merrill AH, Raetz CRH, Russell DW, Subramaniam S, Dennis EA (2010) Subcellular organelle lipidomics in TLR-4-activated macrophages. J Lipid Res 51:2785–2797

Arora-Sharawat A, Chattopadhyay A (2007) Effect of structural transition of the host assembly on dynamics of a membrane-bound tryptophan analogue. Biophys Chem 129:172–180

Baldwin RL (1996) How Hofmeister ion interactions affect protein stability. Biophys J 71:2056–2063

Bangham AD (1972) Model membranes. Chem Phys Lipids 8:386–392

Bansal S, Mittal A (2013) Extracting curvature preferences of lipids assembled in flat bilayers shows possible kinetic windows for genesis of bilayer asymmetry and domain formation in biological membranes. J Membrane Biol 246:557–570

Bansal S, Mittal A (2015) A statistical anomaly indicates symbiotic origins of eukaryotic membranes. Mol Biol Cell 26:1238–1248

Barbosa AM, Santos IJB, Ferreira GMD, da Silva MDH, Teixeira A, da Silva LHM (2010) Microcalorimetric and SAXS determination of PEO-SDS interactions: the effect of cosolutes formed by ions. J Phys Chem B 114:11967–11974

Brini E, Fennell CJ, Fernandez-Serra M, Hribar-Lee B, Lukšic M, Dill KA (2017) How Water's properties are encoded in its molecular structure and energies. Chem Rev 117:12385–12414

Brown DA, London E (1998) Functions of lipid rafts in biological membranes. Annu Rev Cell Dev Biol 14:111–136

Chakraborty H, Sarkar M (2004) Optical spectroscopic and TEM studies of catanionic micelles of CTAB/SDS and their interaction with a NSAID. Langmuir 20:3551–3558

Chaudhuri A, Haldar S, Chattopadhyay A (2009) Organization and dynamics in micellar structural transition monitored by pyrene fluorescence. Biochem Biophys Res Commun 390:728–732

Chaudhuri A, Haldar S, Chattopadhyay A (2012) Structural transition in micelles: novel insight into microenvironmental changes in polarity and dynamics. Chem Phys Lipids 165:497–504

Chernomordik LV, Kozlov MM (2003) Protein-lipid interplay in fusion and fission of biological membranes. Annu Rev Biochem 72:175–207

Chernomordik LV, Kozlov MM, Melikyan GB, Abidor IG, Markin VS, Chizmadzhev YA (1985) The shape of lipid molecules and monolayer membrane fusion. Biochim Biophys Acta 812:643–655

Chernomordik L, Leikina E, Cho M-S, Zimmerberg J (1995) Control of baculovirus gp64-induced syncytium formation by membrane lipid composition. J Virol 69:3049–3058

Christian DA, Tian A, Ellenbroek WG, Levental I, Rajagopal K, Janmey PA, Liu AJ, Baumgart T, Discher DE (2009) Spotted vesicles, striped micelles and Janus assemblies induced by ligand binding. Nat Mater 8:843–849

Christiansson A, Kuypers FA, Roelofsen B, Op Den Kamp JAF, Van Deenen LLM (1985) Lipid molecular shape affects erythrocyte morphology: a study involving replacement of native phosphatidylcholine with different species followed by treatment of cells with sphingomyelinase C or phospholipase A2. J Cell Biol 101:1455–1462

Collins KD (1997) Charge density-dependent strength of hydration and biological structure. Biophys J 72:65–76

Collins KD (2004) Ions from the Hofmeister series and osmolytes: effects on proteins in solution and in the crystallization process. Methods 34:300–311

Cooke IR, Deserno M (2006) Coupling between lipid shape and membrane curvature. Biophys J 91:487–495

Deamer DW (2019) Assembling life: how can life begin on Earth and other habitable planets? Oxford University Press

Dill KA, Bromberg S (2011) Molecular driving forces: statistical thermodynamics in biology, chemistry, physics, and nanoscience, 2nd edn. Garland Science, New York

Dill KA, Truskett T, Vlachy V, Hribar-Lee B (2005) Modeling water, the hydrophobic effect, and ion solvation. Ann Rev Biophys Biomol Struct 34:173–199

Dill KA, Ghosh K, Schmit JD (2011) Physical limits of cells and proteomes. Proc Natl Acad Sci USA 108:17876–17882

Eisenberg D, Kauzmann W (1969) The structure and properties of water. Academic Press, Oxford University Press, Oxford

Ericsson CA, Soderman O, Garamus VM, Bergstrom M, Ulvenlund S (2004) Effects of temperature, salt, and deuterium oxide on the self-aggregation of alkylglycosides in dilute solution. 1. n-nonyl-?-D-glucoside. Langmuir 20:1401–1408

Fennell CJ, Kehoe C, Dill KA (2010) Oil/water transfer is partly driven by molecular shape, not just size. J Am Chem Soc 132:234–240

Ghosh K, Dill KA (2010) Cellular proteomes have broad distributions of protein stability. Biophys J 99:3996–4002

Ghosh K, de Graff AMR, Sawle L, Dill KA (2016) Role of proteome physical chemistry in cell behavior. J Phys Chem B 120:9549–9563

Heinonem JK (2001) Biological role of inorganic phosphate. Springer Science, Business Media, LLC, Berlin

Helenius A, Mccaslin DR, Fries E, Tanford C (1979) Properties of detergents. Meth Enzymol 56:734–749

Imae T, Kamiya R, Ikeda S (1985) Formation of spherical and rod-like micelles of cetyltrimethylammonium bromide in aqueous NaBr solutions. J Colloid Interface Sci 108:215–225

Israelachvili JN, Mitchell DJ, Ninham BWJ (1976) Theory of self-assembly of hydrocarbon amphiphiles into micelles and bilayers. Chem Soc Faraday Trans 72(2):1525–1568

Lahtvee PJ, Sánchez BJ, Smialowska A, Kasvandik S, Elsemman IE, Gatto F, Nielsen J (2017) Absolute quantification of protein and mRNA abundances demonstrate variability in gene-specific translation efficiency in yeast. Cell Syst 4:495–504

Mahler J, Ingmar P (2012) A study of the hydration of the alkali metal ions in aqueous solution. Inorg Chem 51:425–438

Maitra A, Dill KA (2015) Bacterial growth laws reflect the evolutionary importance of energy efficiency. Proc Natl Acad Sci USA 112:406–411

Marcus Y (2009) Effect of ions on the structure of water: structure making and breaking. Chem Rev 109:1346–1370

McMahon HT, Gallop JL (2005) Membrane curvature and mechanisms of dynamic cell membrane remodelling. Nature 438:590–596

Mittal A, Grover RJ (2010) Self-assembly of biological membranes into 200–400 nm aqueous compartments. Nanosci Nanotechnol 10:3085–3090

Mittal A, Jayaram B (2011) The newest view on protein folding: stoichiometric and spatial unity in structural and functional diversity. J Biomol Struct Dyn 28:669–674
Mittal A, Singh S (2018) Insights into eukaryotic evolution from transmembrane domain lengths. J Biomol Struct Dyn 36:2194–2200
Mittal A, Leikina E, Bentz J, Chernomordik LV (2002) Kinetics of influenza hemagglutinin-mediated membrane fusion as a function of technique. Anal Biochem 30:145–152
Mukherjee S, Soe TT, Maxfield FR (1999) Endocytic sorting of lipid analogues differing solely in the chemistry of their hydrophobic tails. J Cell Biol 144:1271–1284
Naresh M, Hasija V, Sharma M, Mittal A (2010) Synthesis of cellular organelles containing nano-magnets stunts growth of magnetotactic bacteria. J Nanosci Nanotechnol 10:4135–4144
Naresh M, Das S, Mishra P, Mittal A (2012) The chemical formula of a magnetotactic bacterium. Biotechnol Bioeng 109:1205–1216
Nelson DL, Cox MM (2008) Lehninger principles of biochemistry, 5th edn. W.H. Freeman & Co Ltd.
Neugebauer JM (1990) Detergents: an overview. Meth Enzymol 182:239–253
Nickolov ZS, Miller JDJ (2005) Water structure in aqueous solutions of alkali halide salts: FTIR spectroscopy of the OD stretching band. Colloid Interface Sci 287:572–580
Poos MI, Costello R, Carlson-Newberry SJ (1999) Institute of Medicine (US) committee on military nutrition research, the role of protein and amino acids in sustaining and enhancing performance. National Academies Press, Washington, DC. https://doi.org/10.17226/9620
Rawat SS, Chattopadhyay A (1999) Structural transition in the micellar assembly: a fluorescence study. J Fluoresc 9:233–244
Ray A, Nemethy G (1971) Effects of ionic protein denaturants on micelle formation by nonionic detergents. J Am Chem Soc 93:6787–6793
Roux A, Cuvelier D, Nassoy P, Prost J, Bassereau P, Goud B (2005) Role of curvature and phase transition in lipid sorting and fission of membrane tubules. EMBO J 24:1537–1545
Sammalkorpi M, Karttunen M, Haataja M (2009) Ionic surfactant aggregates in saline solutions: sodium dodecyl sulfate (SDS) in the presence of excess sodium chloride (NaCl) or calcium chloride (CaCl(2)). J Phys Chem B 113:5863–5870
Santra M, Farrell DW, Dill KA (2017) Bacterial proteostasis balances energy and chaperone utilization efficiently. Proc Natl Acad Sci USA 114:E2654–E2661
Sarkar P, Chattopadhyay A (2015) Dipolar rearrangement during micellization explored using a potential-sensitive fluorescent probe. Chem Phys Lipids 191:91–95
Sarkar P, Chattopadhyay A (2016) Micellar dipole potential is sensitive to sphere-to-rod transition. Chem Phys Lipids 195:34–38
Schafer LV, Marrink SJ (2010) Partitioning of lipids at domain boundaries in model membranes. Biophys J 99:L91–L93
Sezonov G, Joseleau-Petit D, D'Ari R (2007) Escherichia coli physiology in Luria-Bertani broth. J Bacteriol 23:8746–8749
Silverstein KAT, Haymet ADJ, Dill KA (1998) A simple model of water and the hydrophobic effect. J Am Chem Soc 120:3166–3175
Singer SJ, Nicolson GL (1972) The fluid mosaic model of the structure of cell membranes. Science 175:720–731
Singh S, Mittal A (2016) Transmembrane domain lengths serve as signatures of organismal complexity and viral transport mechanisms. Sci Rep 6:22352. https://doi.org/10.1038/srep22352
Singh S, Ponnappan N, Verma A, Mittal A (2019) Osmotic tolerance of avian erythrocytes to complete hemolysis in solute free water. Sci Rep 9:7976. https://doi.org/10.1038/s41598-019-44487-7
Southall NT, Dill KA, Haymet ADJ (2002) A view of the hydrophobic effect. J Phys Chem B 106:521–533

St Vincent MR, Colpitts CC, Ustinov AV, Muqadas M, Joyceb MA, Barsby NL, Epand RF, Epand RM, Khramyshev SA, Valueva OA, Korshun VA, Tyrrell DLJ, Schang LM (2010) Rigid amphipathic fusion inhibitors, small molecule antiviral compounds against enveloped viruses. PNAS 107:17339–17344

Szenk M, Dill KA, de Graff AMR (2017) Why do fast-growing bacteria enter overflow metabolism? Testing the membrane real estate hypothesis. Cell Syst 5:95–104

Tanford C (1973) The hydrophobic effect: formation of micelles and biological membranes, 1st edn. Academic Press, Wiley-Interscience, New York

Tanford C (1978) The hydrophobic effect and the organization of living matter. Science 200:1012–1018

Truskett TM, Dill KA (2003) A simple analytical model of water. Biophys Chem 105:449–459

Urbic T, Dill KA (2017) Analytical theory of the hydrophobic effect of solutes in water. Phys Rev E 96:32101

Urbic T, Dill KA (2018) Water Is a Cagey Liquid. J Am Chem Soc 140:17106–17113

Urbic T, Vlachy V, Kalyuzhnyi YV, Dill KA (2007) Theory for the solvation of nonpolar solutes in water. J Chem Phys 127:174505

Van Meer G, Voelker DR, Feigenson GW (2008) Membrane lipids: where they are and how they behave. Nat Rev Mol Cell Biol 9:112–124

Voet D, Voet JG, Pratt CW (2013) Principles of biochemistry. Wiley, New York

Wagoner J, Dill KA (2019) Mechanisms for achieving high speed and efficiency in biomolecular machines. Proc Natl Acad Sci USA 116:5902–5907

Wetlaufer DB, Malik SK, Stoller L, Coffin RL (1964) Nonpolar group participation in the denaturation of proteins by urea and guanidinium salts. Model compound studies. J Am Chem Soc 86:508–514

Xu H, Dill KA (2005) Water's hydrogen bonds in the hydrophobic effect: a simple model. J Phys Chem B 109:23611–23617

Yang L, Liao R-Z, Yu J-G, Liu R-Z (2009) DFT study on the mechanism of *Escherichia coli* inorganic pyrophosphatase. J Phys Chem B 113:6505–6510

Zaitseva E, Yang ST, Melikov K, Pourmal S, Chernomordik LV (2010) Dengue virus ensures its fusion in late endosomes using compartment-specific lipids. PLoS Pathog 6:e1001131

Zhang JZ (2000) Protein-length distributions for the three domains of life. Trends Genet 16:107–109

Zhang Y, Cremer PS (2006) Interactions between macromolecules and ions: The Hofmeister series. Curr Opin Chem Biol 10:658–663

Zimmerberg J, Kozlov MM (2006) How proteins produce cellular membrane curvature. Nature Rev Mol Cell Biol 7:9–19